Research Article

1,3,4-Thiadiazole Analogues Targeting EGFR: Docking, *in Silico* ADME, Synthesis and Cytotoxicity Against A549 Lung Cancer Cells

Hemant Vishnu Dhakne[1] , Dr. Archana Shriram Gurjar[2*]

[1]M. Pharm., Ph. D. Research Scholar, Department of Pharmaceutical Chemistry, Principal K. M. Kundnani College of Pharmacy, Mumbai-400 005, Maharashtra, India. ORCID: https://orcid.org/0009-0006-4135-283X
[2]Ph.D. (Tech.) in Pharmaceutical Chemistry, Assistant Professor (Senior Scale), Department of Pharmaceutical Chemistry and Pharmaceutical Analysis, Principal K. M. Kundnani College of Pharmacy, Mumbai-400 005, Maharashtra, India. ORCID: https://orcid.org/0000-0002-3352-3567

Correspondence Author:
*Dr. Archana Shriram Gurjar, E-mail: as.gurjar@kmkcp.edu.in

ABSTRACT

Non-small cell lung cancer is a type which accounts for nearly 85% of lung cancers and EGFR tyrosine kinase inhibitors (TKIs) are the most common available treatment options. Amongst the EGFR-mutations C797S is the latest of these resistance mutations, which outsmarts multiple generations of these inhibitors, and no therapy has been approved. Inhibitors EAI001 and EAI045 fill this void, and both possess N-(thiazol-2-yl) acetamide moiety. From the literature inputs, a series of 1,3,4-thiadiazole analogues was designed, docked and validated using Protein Data Bank ID: 1M17 with root mean square deviation of 0.896 Å for the co-crystallized erlotinib. The binding energies for analogues were in the range of −8.14 to −9.85 kcal/mol, which were favorable than redocked erlotinib (−7.78 kcal/mol). All analogues exhibited hydrogen bond interactions with hinge residue Met769. Most of them obeyed Lipinski's rule of five calculated utilizing SwissADME. For the synthesis, corresponding carboxylic acids were cyclocondensed with thiosemicarbazide in phosphorus oxychloride at 80–90 °C to form 5-substituted-1,3,4-thiadiazol-2-amines. The structures identity were confirmed by spectral techniques. Four analogues showed promising reduced viability of less than 50% at 1000 µg/mL at 72 h in the 3-(4,5-dimethylthiazol-2-yl)-2,5-diphenyltetrazolium bromide assay against A549 cells. The T3 (26.30%), T1 (40.10%), T4 (42.23%) and T10 (48.67%) showcased IC_{50} values of 4.12, 7.7, 3.96 and 3.97 mM with respect to erlotinib: 1.66 mM for cell growth inhibition. The analogues were moderately cytotoxic and the T4 was the most active analogue. T4 and T3 analogues possess potential for further structural optimization.

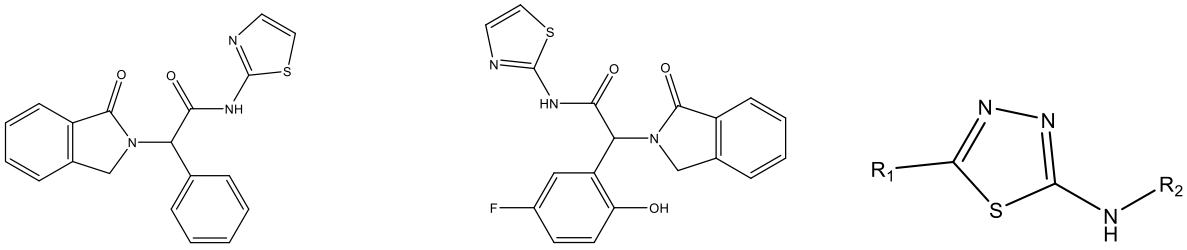
Keywords: 1,3,4-Thiadiazole; A549 cells; EGFR; Molecular docking; Non-small cell lung cancer; SwissADME

1. INTRODUCTION

Worldwide, an estimated 20.6 million new cancer cases and 9.8 million cancer deaths occurred in 2024, and lung cancer ranked first in both incidence (about 2.6 million cases, 12.8%) and mortality (about 1.9 million deaths, 19.1%).[1] Non–small cell lung cancer (NSCLC) accounts for ~85% of lung cancers.[2] India also bears a heavy burden of cancer, with an estimated 1,562,581 new cases and 901,828 deaths in 2024. Lung cancer (112,659 new cases and 98,687 deaths) is the leading cause of cancer death in India and the second most common cancer in Indian men. The epidermal growth factor receptor called (EGFR/ErbB1) is a cell surface receptor tyrosine kinase.[3] Ligand engagement induces receptor dimerization and autophosphorylation of the intracellular kinase domain, activating the RAS-RAF-MEK-ERK and PI3K-AKT-mTOR pathways that promote cell proliferation, survival and metastasis.[4] Activating mutations, mainly

deletions in exon 19 and the L858R mutation in exon 21, render NSCLC tumors dependent on and sensitive to EGFR signaling and EGFR TKIs.[5] Resistance is frequently driven by acquisition of the T790M "gatekeeper" mutation.[6,3] Inhibition of wild-type EGFR limited the toxicity of second-generation irreversible inhibitors. Third-generation inhibitors bind covalently to cysteine 797 and overcome T790M. The C797S mutation causes acquired resistance by eliminating the binding site for third-generation inhibitors.[7] there is currently no approved therapy that targets EGFR with the C797S mutation.[8] Researchers are developing fourth-generation EGFR inhibitors to fill this gap. EAI001 and EAI045 are the first mutant-selective allosteric EGFR inhibitors Figure 1. They bind to a pocket adjacent to the ATP site, created by displacement of the regulatory αC-helix. They inhibit the L858R/T790M mutant at nanomolar concentrations, but not wild-type EGFR, and EAI045 plus an EGFR-blocking antibody was effective in mouse models driven by L858R/T790M/C797S EGFR.[9] EAI001 inhibited the L858R/T790M mutant with an IC_{50} of 24 nM with more than 50 μM for wild-type EGFR and the optimized analogue EAI045 was even more potent with an IC_{50}: 3 nM for L858R/T790M and 4.3 μM for the wild-type enzyme a selectivity window of about 1000-fold.[9] There are several candidates in this research development, but none has yet been approved.[8] A549 cells, established from human lung adenocarcinoma,[10] are standard for NSCLC model; because they combine wild-type EGFR with mutant KRAS, they respond poorly to EGFR TKIs.[11,12] Activity in this line thus constitutes a rigorous test for novel EGFR-directed agents.[9] Both EAI001 and EAI045 share an N-(thiazol-2-yl) acetamide moiety, with the thiazole ring contributing to binding to EGFR. Therefore, we speculated that 1,3,4-thiadiazole derivatives, based on the heterocyclic characteristics of these fourth-generation inhibitors, could interact with the EGFR kinase domain and inhibit NSCLC cell growth. Figure 1 shows the design strategy.

(a) **(b)** **(c)**



EAI001 **EAI045** **Design scaffold**

Figure 1. Fourth-generation EGFR inhibitors: a. EAI001, b. EAI045 and c. Scaffold for design of 2,5-disubstituted 1,3,4-thiadiazole analogues.

To analyze this theory, we designed a series of 1,3,4-thiadiazole analogues, docked them within the EGFR kinase domain, and profiled them for drug-likeness properties. The analogues were then synthesized, characterized by spectral analysis and screened for cytotoxicity against A549 cells by the MTT assay, with a clinically used EGFR inhibitor as the reference standard, to identify promising structures for further optimization.

2. MATERIALS AND METHODS

2.1 General

Computational work was carried out with ChemDraw Professional version 22.0 (PerkinElmer, Waltham, MA, USA), UCSF Chimera version 1.17.3 for protein preparation, AutoDockTools

version 1.5.7, AutoDock Vina version 1.1.2 for docking, SwissADME, BIOVIA Discovery Studio Visualizer version 21.1.0 and PyMOL version 2.5.7 and GraphPad Prism version 10.1.1 for curve fitting and statistical analysis.

Reagents and solvents were acquired from different vendors. The reaction progress was observed by using thin layer chromatography (TLC) silica gel 60 F_{254} aluminium plates (Merck KGaA, Darmstadt, Germany) using ethyl acetate: n-hexane (3:7, v/v) and chloroform: methanol (9:1, v/v) for the 2-amino-1,3,4-thiadiazoles and n-hexane: ethyl acetate (8:2, v/v) or chloroform for the sulfonamide. Melting points (open capillary, Thiele tube) are uncorrected. Infrared spectra as KBr pellets on Bruker FTIR spectrometer (ALPHA II). The ^{1}H NMR spectra were documented on Bruker 400 MHz NMR spectrometer (Bruker Avance III) spectrometer at 400 MHz using DMSO-d_6 ($CDCl_3$ for T11) as solvent and tetramethyl silane (TMS) as an internal reference.

2.2 Molecular Docking

For docking the EGFR kinase domain co-crystallized with erlotinib (PDB ID: 1M17; 2.60 Å), was employed. [13]. Analogue structures were sketched in ChemDraw Professional. The Dock Prep tool of UCSF Chimera was used to clean the receptor (removal of water, the native ligand and other heteroatoms; repair of incomplete side chains; addition of hydrogens and charges). Receptor and ligands were then minimized with Chimera's default routine, applying ff14SB to the protein[15] and GAFF parameters with AM1-BCC charges to the ligands.[14,] AutoDockTools merged non-polar hydrogens, added Gasteiger charges and wrote the PDBQT files; ligand torsions were free and the protein was rigid. AutoDock Vina was run at an exhaustiveness of 8 in a 10 × 10 × 10 Å box centred on native erlotinib (x = 22.013, y = 0.252, z = 52.794), spanning the hinge Met769, the gatekeeper Thr766 and the neighbouring Leu694, Ala719, Lys721 and Leu820;[16] the lowest-energy pose of each ligand was retained. To validate the set-up for this study, erlotinib was removed from 1M17 and redocked.. Poses and 2D interaction maps were examined in Discovery Studio Visualizer and PyMOL.

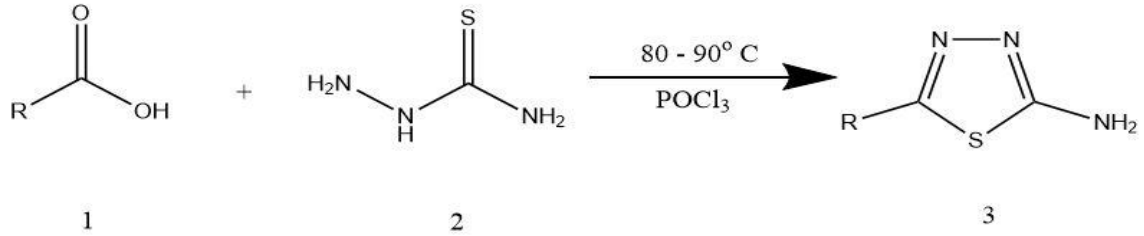
2.3 *In Silico* ADME and Drug-Likeness Prediction

Descriptors were calculated on the SwissADME server from SMILES of the ChemDraw structures. [17]

2.4 Chemistry

2.4.1 General procedure for 5-substituted-1,3,4-thiadiazol-2-amines

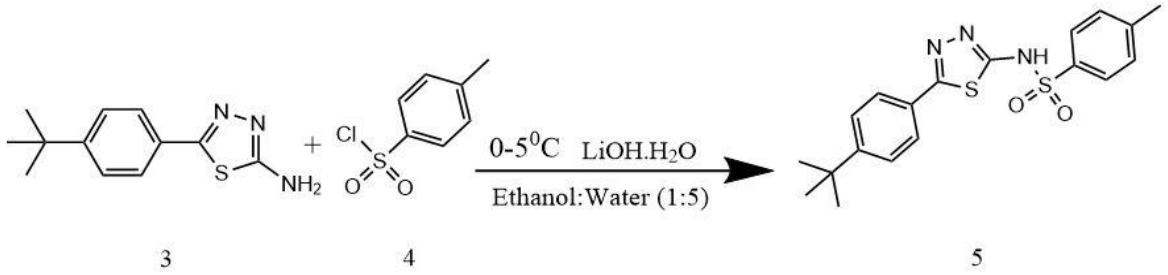
The chosen carboxylic acid (**1**, 0.1 mol) and thiosemicarbazide (**2**, 0.1 mol) were charged into dry round-bottom flask, phosphorus oxychloride (30 mL, ~0.32 mol) was added dropwise at ambient temperature, and the mixture was heated to 80–90 °C for 3–4 h utilizing TLC to monitor the completion of reaction (Scheme 1). Once cooled, ice-cold water (200 mL) was added with care, and pH was adjusted to 8 with 10% sodium hydroxide. [18] The precipitate was collected by vacuum filtration, rinsed with cold water, dried and recrystallized from aqueous ethanol. The structures were confirmed by IR and ^{1}H NMR spectroscopy.



Scheme 1. Synthesis of 5-substituted-1,3,4-thiadiazol-2-amines (3) from substituted carboxylic acids (1) and thiosemicarbazide (2) in phosphorus oxychloride.

2.4.2 Synthesis of N-[5-(4-tert-butylphenyl)-1,3,4-thiadiazol-2-yl]-4-methylbenzenesulfonamide (6) (T11)

5-(4-*tert*-Butylphenyl)-1,3,4-thiadiazol-2-amine (**3**; 1.17 g, 5.0 mmol) and lithium hydroxide monohydrate (0.210 g, 5.0 mmol) were stirred in ethanol (3 mL) at 0–5 °C until dissolved. 4-Methylbenzenesulfonyl chloride (**4**; 0.953 g, 5.0 mmol) and water (15 mL) were added, resulting an ethanol: water ratio of 1:5, and the mixture was stirred vigorously at 0–5 °C for 2–3 h with a calcium chloride guard tube (Scheme 2).[19]



Scheme 2. Synthesis of *N*-[5-(4-*tert*-butylphenyl)-1,3,4-thiadiazol-2-yl]-4-methylbenzenesulfonamide (5).

2.5 Characterization data of the synthesized compounds

2.5.1 5-Methyl-1,3,4-thiadiazol-2-amine (T1)

Yield: 80%; appearance: white solid; m.p.: 228 °C; Rf: 0.67 (EtOAc : n-hexane, 3:7); Rf: 0.70 ($CHCl_3$: MeOH, 9:1); mol. formula: $C_3H_5N_3S$ (MW 115.15). IR (KBr, νmax, cm^{-1}): 3300–3100 (N–H asym./sym. str., NH_2), 2980–2920 (C–H str., CH_3), , 1530–1500 (C=N str., thiadiazole), 1080–1040 (N–N str.), 700–650 (C–S–C str., thiadiazole). ^{1}H NMR (400 MHz, DMSO-d_6) δ (ppm): 6.96 (s, 2H, NH_2), 2.43 (s, 3H, CH_3); residual DMSO at δ 2.50 and H_2O at δ 3.35.

2.5.2 5-Phenyl-1,3,4-thiadiazol-2-amine (T2)

Yield: 80%; appearance: white solid; m.p.: 224 °C; Rf: 0.58 (EtOAc : n-hexane, 3:7); Rf: 0.62 ($CHCl_3$: MeOH, 9:1); mol. formula: $C_8H_7N_3S$ (MW 177.22). IR (KBr, νmax, cm^{-1}): 3300–3100 (N–H asym./sym. str., NH_2), 3080–3030 (aromatic C–H str.), 1530–1490 (C=N / C–N str., thiadiazole), 1470–1440 (aromatic C=C str.), 1080–1040 (N–N str.), 770–750 and 700–680 (C–H oop bend, monosubstituted ring), 690–650 (C–S–C str.). ^{1}H NMR (400 MHz, DMSO-d_6) δ (ppm): 7.77–7.75 (m, 2H, H-2′, H-6′), 7.53–7.43 (m, 5H, H-3′, H-4′, H-5′ and NH_2, overlapping); residual DMSO at δ 2.50 and H_2O at δ 3.36.

2.5.3 5-(Trifluoromethyl)-1,3,4-thiadiazol-2-amine (T3)

Yield: 82%; appearance: white solid; m.p.: 225 °C; Rf: 0.68 (EtOAc : n-hexane, 3:7); Rf: 0.72 ($CHCl_3$: MeOH, 9:1); mol. formula: $C_3H_2F_3N_3S$ (MW 169.12). IR (KBr, νmax, cm^{-1}): 3303, 3129 (N–H asym./sym. str., NH_2), 1515 (C=N str.), 1190, 1150 (C–F str., CF_3), 1040 (N–N str.) cm^{-1}. ^{1}H NMR (400 MHz, DMSO-d_6) δ (ppm): 8.05 (s, 2H, NH_2); residual DMSO at δ 2.50 and H_2O at δ 3.36.

2.5.4 5-(4-(tert-Butyl)phenyl)-1,3,4-thiadiazol-2-amine (T4)

Yield: 95%; appearance: white solid; m.p.: 215 °C; Rf: 0.45 (EtOAc : n-hexane, 3:7); Rf: 0.55 ($CHCl_3$: MeOH, 9:1); mol. formula: $C_{12}H_{15}N_3S$ (MW 233.33). IR (KBr, νmax, cm^{-1}): 3280.40, 3101.55 (N–H asym./sym. str., NH_2), 2957.18 (C–H asym. str., $C(CH_3)_3$), 2902.00, 2866.29 (C–H sym. str., CH_3), 1564.81,1510 (aromatic C=C str.), 1265.30 (C–N str.), 1055.66 (N–N str., thiadiazole), 691.74 (C–S–C str., thiadiazole). ^{1}H NMR (400 MHz, DMSO-d_6) δ (ppm): 7.68 (d,

J = 8.3 Hz, 2H, H-2′, H-6′), 7.48 (d, J = 8.3 Hz, 2H, H-3′, H-5′), 7.36 (br s, 2H, NH_2), 1.30 (s, 9H, $C(CH_3)_3$); residual DMSO at δ 2.50 and H_2O at 3.37

2.5.5 2-(5-Amino-1,3,4-thiadiazol-2-yl)benzoic acid (T5)

Yield: 70%; appearance: yellow solid; m.p.: 232 °C; Rf: 0.54 (EtOAc : n-hexane, 3:7); Rf: 0.60 ($CHCl_3$: MeOH, 9:1); mol. formula: $C_9H_7N_3O_2S$ (MW 221.23). IR (KBr, νmax, cm^{-1}): 3400, 3260 (NH_2), 3080 (Ar C–H), 3000–2500 (broad O–H, COOH), 1685 (C=O), 1615 (C=N), 1500 (C=C), 1290 (C–O), 1065 (N–N), 920 (O–H oop), 760 (ortho C–H oop), 680 (C–S–C).^{1}H NMR (400 MHz, DMSO-d_6) δ (ppm): 8.50 (d, H-11), 8.19–8.14 (m, H-8, H-10),7.89–7.86 (m, H-9), 7.69–7.62 (d, J = 12 Hz, H-2); residual DMSO at δ 2.53.

2.5.6 3-(5-Amino-1,3,4-thiadiazol-2-yl)benzoic acid (T6)

Yield: 70%; appearance: yellow solid; m.p.: 225 °C; Rf: 0.60 (EtOAc : n-hexane, 3:7); Rf: 0.54 ($CHCl_3$: MeOH, 9:1); mol. formula: $C_9H_7N_3O_2S$ (MW 221.23). IR (KBr, νmax, cm^{-1}): 3428.94, 3258.33 (N–H asym./sym. str., NH_2), 3085.42 (aromatic C–H str.), 2887.42, 2821.22, 2661.40, 2545.05 (broad O–H str., H-bonded COOH dimer), 1684.30 (C=O str., aromatic carboxylic acid), 1498.22 (aromatic C=C str.), 1295.77 (C–O str., COOH), 1068.44 (N–N str., thiadiazole), 925.86 (O–H oop bend, acid dimer), 845.62 (C–H oop bend, isolated H-2′), 673.66 (C–S–C str., thiadiazole). ^{1}H NMR (400 MHz, DMSO-d_6) δ (ppm): 8.38 (d, H-11), 8.29–8.24 (m, H-8, H-10), 7.79–7.76 (m, H-9), 7.59–7.52 (d, J = 12 Hz, H-2); residual DMSO at δ 2.55.

2.5.7 5-((1H-Indol-3-yl) methyl)-1,3,4-thiadiazol-2-amine (T7)

Yield: 55%; appearance: brown solid; m.p.: 235 °C; Rf: 0.47 (EtOAc : n-hexane, 3:7); Rf: 0.70 ($CHCl_3$: MeOH, 9:1); mol. formula: $C_{11}H_{10}N_4S$ (MW 230.29). IR (KBr, νmax, cm^{-1}): 3276.31 (N–H str., indole NH and NH_2, H-bonded), 3056.11 (aromatic C–H str.), 2920.70, 2852.53 (C–H asym./sym. str., CH_2), 1622.52 (C=N str., thiadiazole), 1515.08, 1488.40 (aromatic C=C str.), 1455.37 (CH_2 scissoring / aromatic C=C str.), 1337.78, 1224.67 (C–N str.), 1068.48 (N–N str., thiadiazole), 709.45 (C–S–C str., thiadiazole). ^{1}H NMR (400 MHz, DMSO-d_6) δ (ppm): 11.08 (s, 1H, indole N–H), 7.47 (d, J = 7.6 Hz, 1H, H-4), 7.38 (d, J = 8.1 Hz, 1H, H-7), 7.32 (s, 1H, H-2), 7.10 (t, J = 7.6 Hz, 1H, H-6), 6.99 (t, J = 7.6 Hz, 1H, H-5), 4.27 (s, 2H, CH_2); NH_2 not resolved (broad exchange hump with H_2O at δ 4.8–5.7); residual DMSO at δ 2.50.

2.5.8 3-amino-4-(5-amino-1,3,4-thiadiazol-2-yl)phenol (T8)

Yield: 50%; appearance: black solid; m.p.: 242 °C; Rf: 0.72 (EtOAc : n-hexane, 3:7); Rf: 0.55 ($CHCl_3$: MeOH, 9:1); mol. formula: $C_8H_8N_4OS$ (MW 208.24). IR (KBr, νmax, cm^{-1}): 3486.34, 3381.34 (N–H asym./sym. str., aryl NH_2), 3218.52 (N–H str., thiadiazole NH_2 / O–H str.), 3050.57 (aromatic C–H str.), 2868.26, 2620.12, 2578.74 (broad, intramolecularly H-bonded O–H/N–H str.), 1602.10 (C=N str., thiadiazole, overlapped with N–H bend), 1489.61, 1447.80 (aromatic C=C str.), 1342.05, 1288.17 (aryl C–N str.), 1231.30 (phenolic C–O str.), 1053.37 (N–N str., thiadiazole), 838.77 (C–H oop bend, 1,2,4-trisubstituted ring), 682.07 (C–S–C str., thiadiazole). ^{1}H NMR (400 MHz, DMSO-d_6) δ (ppm): 7.42 (d, J = 8.3 Hz, 1H, H-3), 6.18 (br s, 2H, Ar–NH_2), 6.10 (dd, J = 8.3, Hz, 1H, H-4), 5.98 (s, 1H, H-6), 4.97 (br, OH and thiadiazole NH_2, exchanging with H_2O); residual DMSO at δ 2.50.

2.5.9 (E)-5-(2-(5-Amino-1,3,4-thiadiazol-2-yl)vinyl)-2-methoxyphenol (T9)

Yield: 85%; appearance: yellow powder; m.p.: 234 °C; Rf: 0.49 (EtOAc : n-hexane, 3:7); Rf: 0.72 ($CHCl_3$: MeOH, 9:1); mol. formula: $C_{11}H_{11}N_3O_2S$ (MW 249.29). IR (KBr, νmax, cm^{-1}): 3347.41 (O–H and N–H str., H-bonded), 2942.20 (C–H str., OCH_3), 1629.45 (C=N str., thiadiazole), 1593.86 (C=C str., conjugated vinyl / N–H bend), 1507.90 (aromatic C=C str.), 1268.62 (C–O–C asym. str., aryl methyl ether), 1209.24 (phenolic C–O str.), 1077.41 (N–N str., thiadiazole), 1026.37 (C–O–C sym. str.), 709.90 (C–S–C str., thiadiazole). ^{1}H NMR (400 MHz,

DMSO-d_6) δ (ppm): 7.79 (br s, 2H, NH_2), 7.38–7.02 (m, 4H, H-α, H-β, H-2′, H-6′), 6.79 (d, J = 8.3 Hz, 1H, H-5′), 5.10 (br s, 1H, OH), 3.82 (s, 3H, OCH_3); residual DMSO at δ 2.50.

2.5.10 5-(4-Nitrobenzyl)-1,3,4-thiadiazol-2-amine (T10)

Yield: 92%; appearance: white solid; m.p.: 218 °C; Rf: 0.63 (EtOAc : n-hexane, 3:7); Rf: 0.62 ($CHCl_3$: MeOH, 9:1); mol. formula: $C_9H_8N_4O_2S$ (MW 236.25). IR (KBr, νmax, cm^{-1}): 3399.83, 3278.72 (N–H asym./sym. str., NH_2), 3108.51, 3073.09 (aromatic C–H str.), 1638.06 (C=N str., thiadiazole / N–H bend), 1600.88 (aromatic C=C str.), 1520 (NO_2 asym. str.), 1425.22 (CH_2 scissoring), 1345 (NO_2 sym. str.), 1106.21 (C–N str.), 1042.61 (N–N str., thiadiazole), 858.63 (C–H oop bend, para-disubstituted ring), 748.86 (NO_2 bend), 699.39 (C–S–C str., thiadiazole). ^{1}H NMR (400 MHz, DMSO-d_6) δ (ppm): 8.21 (d, J = 8.3 Hz, 2H, H-3′, H-5′), 7.90 (br s, 2H, NH_2), 7.59 (d, J = 8.3 Hz, 2H, H-2′, H-6′), 4.37 (s, 2H, CH_2); residual DMSO at δ 2.50.

2.511 N-(5-(4-(tert-Butyl)phenyl)-1,3,4-thiadiazol-2-yl)-4-methylbenzenesulfonamide (T11)

Yield: 50%; appearance: yellow powder; m.p.: 211 °C; Rf: 0.58 (EtOAc : n-hexane, 3:7); Rf: 0.60 ($CHCl_3$: MeOH, 9:1); mol. formula: $C_{19}H_{21}N_3O_2S_2$ (MW 387.52). IR (KBr, νmax, cmIR (cm^{-1}): 3200 (N–H, SO_2NH), 3060 (Ar C–H), 2960, 2870 (tert-butyl C–H), 2925 (Ar–CH_3), 1595 (C=N), 1510, 1490 (C=C), 1335 (S=O asym.), 1155 (S=O sym.), 1060 (N–N), 915 (S–N), 830, 815,690 (C–S–C),.^{1}H NMR (400 MHz, $CDCl_3$) δ (ppm): 7.80 (d, J = 8.3 Hz, 2H, tosyl H-2″, H-6″), 7.73 (d, J = 8.7 Hz, 2H, H-2′, H-6′), 7.45 (d, J = 8.7 Hz, 2H,H-3′, H-5′), 7.34 (d, J = 8.3 Hz, 2H, tosyl H-3″, H-5″), 5.53 (s, 1H, SO_2NH), 2.45 (s, 3H, Ar–CH_3), 1.34 (s, 9H, $C(CH_3)_3$); residual $CHCl_3$ at δ 7.26. The absence of the NH_2 signal of T4 confirms N-sulfonylation.

2.6 *In Vitro* Cytotoxicity Assay

A549 cells from the National Centre for Cell Science, Pune, India, were grown in Dulbecco's Modified Eagle Medium (DMEM) with 10% fetal bovine serum at 37 °C under 5% CO_2. Compounds (10 mg) were dissolved in 100 µL dimethyl sulfoxide and made up to 1000 µg/mL in DMEM with 1% serum, filtered (0.45 µm) and halved stepwise to 62.5 µg/mL. Erlotinib (1.97–1229.5 µg/mL) served as reference. Cells were seeded at 8×10^3 per well (1×10^4 for erlotinib), left 24 h to attach and treated for 72 h in triplicate. MTT was added for 4 h, the formazan dissolved in acidified isopropanol and absorbance read at 570 nm on a Cytation 5 reader; wells were photographed at 20×. Viability was calculated against untreated controls and IC_{50} fitted by nonlinear regression in GraphPad Prism v10.1.1. Values are mean ± SD (n = 3), compared by one-way ANOVA with Dunnett's test ($p < 0.05$).

3. RESULTS AND DISCUSSION

3.1 Molecular Docking

Redocking of erlotinib returned the crystallographic posture with an RMSD of 0.896 Å (Figure 2), showing that the docking protocol reproduces an empirically observed binding mode. From the designed series, the eleven synthesized analogues were bound in the ATP-binding region with projected binding energies ranging from −8.14 (T1) to −9.85 (T4) kcal/mol, higher than erlotinib (−7.78 kcal/mol) (Table 1). The best was T4, followed by the N-tosyl sulfonamide T11 (−9.44 kcal/mol) and the 5-trifluoromethyl counterpart T3 (−9.11 kcal/mol).

In the crystal structure, the quinazoline N1 of erlotinib accepts a hydrogen bond from the backbone NH of Met769. All eleven analogues also hydrogen-bonded to Met769, suggesting that the 2-amino-1,3,4-thiadiazole ring takes the place of the quinazoline at the hinge (Figure 2). T3, T11, and several other analogues formed an additional hydrogen bond with the gatekeeper residue Thr766. The bulky, lipophilic 4-*tert*-butylphenyl group shared by T4 and T11 probably contributes hydrophobic contacts within the pocket.

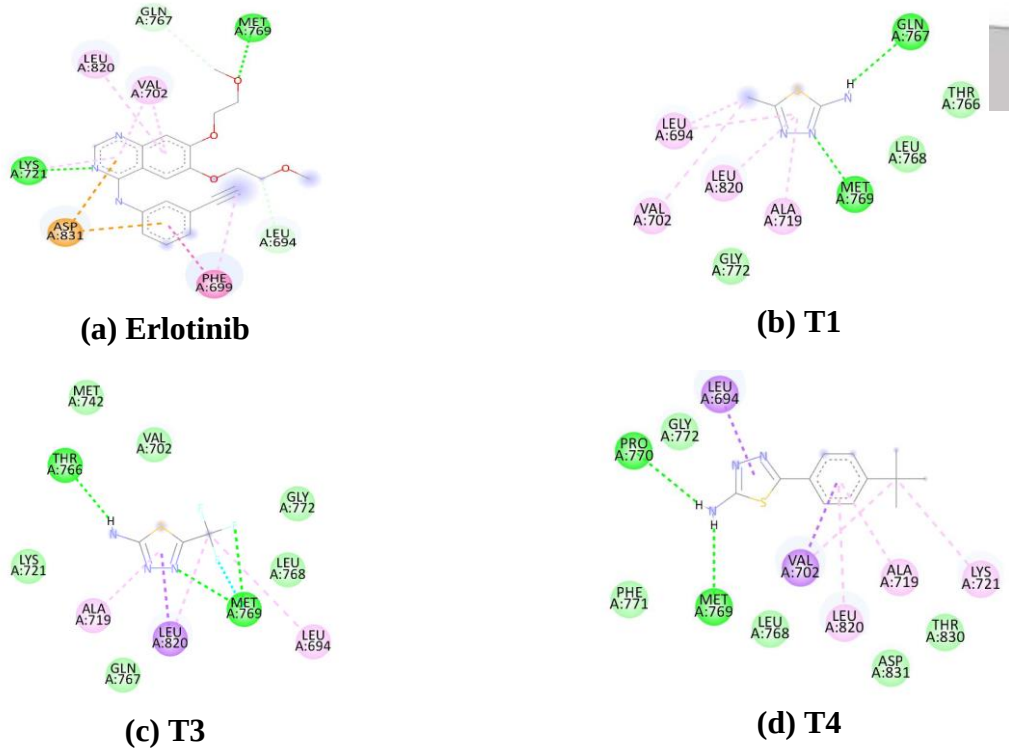
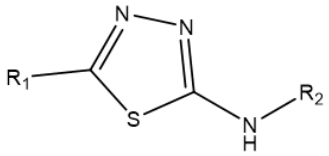


Figure 2. Representative docking poses within the ATP-binding site of EGFR (PDB ID: 1M17): (a) erlotinib, (b) T1, (c) T3, and (d) T4.

Table 1. Molecular docking results of the 1,3,4-thiadiazole analogues



Sr. no.	Code	R1	R2	Hydrogen bonds with active-site residues	Binding energy (kcal/mol)
—	Erlotinib	—	—	Met769, Cys773	−7.78
1	T1	$–CH_3$	H	Met769, Gln767	−8.14
2	T2	$–C_6H_5$	H	Met769	−8.52
3	T3	$–CF_3$	H	Met769, Thr766	−9.11
4	T4	p-$(CH_3)_3C–C_6H_4–$	H	Met769, Pro770	−9.85
5	T5	o-COOH–$C_6H_4–$	H	Met769, Thr766	−8.92
6	T6	m-COOH–$C_6H_4–$	H	Met769, Thr766, Gln767	−8.47
7	T7	Indol-3-yl–$CH_2–$	H	Met769, Asp831	−8.36
8	T8	o-NH_2,p-OH,$C_6H_3–$	H	Met769, Gln767, Leu694, Thr766	−8.55
9	T9	p-OH, m-$OCH_3C_6H_3$-CH=CH-	H	Met769, Asp831, Arg817	−8.28

Sr. no.	Code	R1	R2	Hydrogen bonds with active-site residues	Binding energy (kcal/mol)
10	T10	p-NO_2–CH_2–C_6H_4–	H	Met769, Thr766	−8.87
11	T11	p-$(CH_3)_3C$–C_6H_4–	p-methyl–C_6H_4–SO_2–	Met769, Thr766	−9.44

3.2 ***In Silico*** **ADME and Drug-Likeness**

The analogues are small molecules (115.16–387.52 g/mol) with two to five hydrogen-bond acceptors and one to three donors, and none violates Lipinski's rule of five (Table 2). Full form (TPSA) values (80.04–126.29 Å^2) are below the 130 Å^2 limit, and consensus log $P_{o/w}$ values (0.54–4.21) fall within the accepted range. Gastrointestinal absorption was predicted high for every compound except T11, the most lipophilic member of the series (log $P_{o/w}$ 4.21), which also showed the poorest predicted aqueous solubility (ESOL log *S* −5.24). Bioavailability scores were 0.55 throughout, except for erlotinib (0.56) and the carboxylic acids T5 and T6, and synthetic accessibility (2.43–2.94; 3.75 for T11) was below that of erlotinib (3.19), consistent with the short route used.

Table 2. *In silico* ADME and drug-likeness properties of the 1,3,4-thiadiazole analogues

Code	MW	HBA	HBD	TPSA	Cons. log $P_{o/w}$	ESOL log *S*	GI abs.	Lipinski viol.	Bioavail. score	Synth. Access.
SwissADME range	< 500	≤ 10	≤ 5	≤ 130	−0.7 to 5	0 ≥ −6	—	0–2	0–1	1–10
Erlotinib	393.44	6	1	74.73	3.39	−4.83	High	0	0.55	3.19
T1	115.16	2	1	80.04	0.54	−1.32	High	0	0.55	2.48
T2	177.23	2	1	80.04	1.85	−2.61	High	0	0.55	2.46
T3	169.13	5	1	80.04	1.45	−1.78	High	0	0.55	2.43
T4	233.33	2	1	80.04	2.98	−3.77	High	0	0.55	2.69
T5	221.24	4	2	117.34	1.30	−2.38	High	0	0.56	2.64
T6	221.24	4	2	117.34	1.12	−2.38	High	0	0.56	2.65
T7	230.29	2	2	95.83	1.89	−3.11	High	0	0.55	2.50
T8	208.24	3	3	126.29	0.81	−2.05	High	0	0.55	2.60
T9	249.29	4	2	109.50	1.79	−2.89	High	0	0.55	2.94
T10	236.25	4	1	125.86	1.20	−2.75	High	0	0.55	2.53
T11	387.52	4	1	108.57	4.21	−5.24	Low	0	0.55	3.75

MW, molecular weight (g/mol); TPSA in Å²; HBA, hydrogen-bond acceptors; HBD, hydrogen-bond donors; TPSA, topological polar surface area (Å^2); GI, gastrointestinal; Synthetic accessibility is scored from 1 (easy) to 10 (difficult).

3.3 Chemistry

The analogues were synthesized using Schemes 1 and 2. Cyclocondensation of the appropriate carboxylic acid with thiosemicarbazide in excess $POCl_3$ at 80–90 °C gave T1–T10, with $POCl_3$ acting as both an activating and dehydrating agent: it promotes acylation of thiosemicarbazide, and the resulting acylthiosemicarbazide cyclodehydrates to the thiadiazole ring. Quenching with ice-cold water hydrolyzed residual reagent, and basification to pH 8 liberated the free bases from their hydrochloride salts. *N*-Sulfonylation of T4 with 4-methylbenzenesulfonyl chloride and 1 equiv. $LiOH·H_2O$ in ethanol: water (1:5) at 0–5 °C gave T11 in 50% yield, m.p. 211 °C; the low

temperature limits competing hydrolysis of the sulfonyl chloride, and the product precipitated directly from the reaction mixture.

All the structures were confirmed by IR and ^{1}H NMR spectroscopy. For T1–T10, the two NH_2 stretching bands were observed between 3430–3100 cm^{-1} and the thiadiazole C=N stretch at 1640–1490 cm^{-1}. In most of the proton NMR, the NH_2 protons appeared as a broad singlet at δ 6.96–8.05 ppm Three changes in NMR confirmed T11 formation: the NH_2 signal was replaced by a one-proton sulfonamide N–H singlet at δ 5.53 ppm, two SO_2 stretching bands appeared near 1335 and 1155 cm^{-1}, and a three-proton aryl-CH_3 singlet at δ 2.45 ppm accompanied the nine-proton *tert*-butyl singlet at δ 1.34 ppm.

3.4 Cytotoxicity against A549 Cells

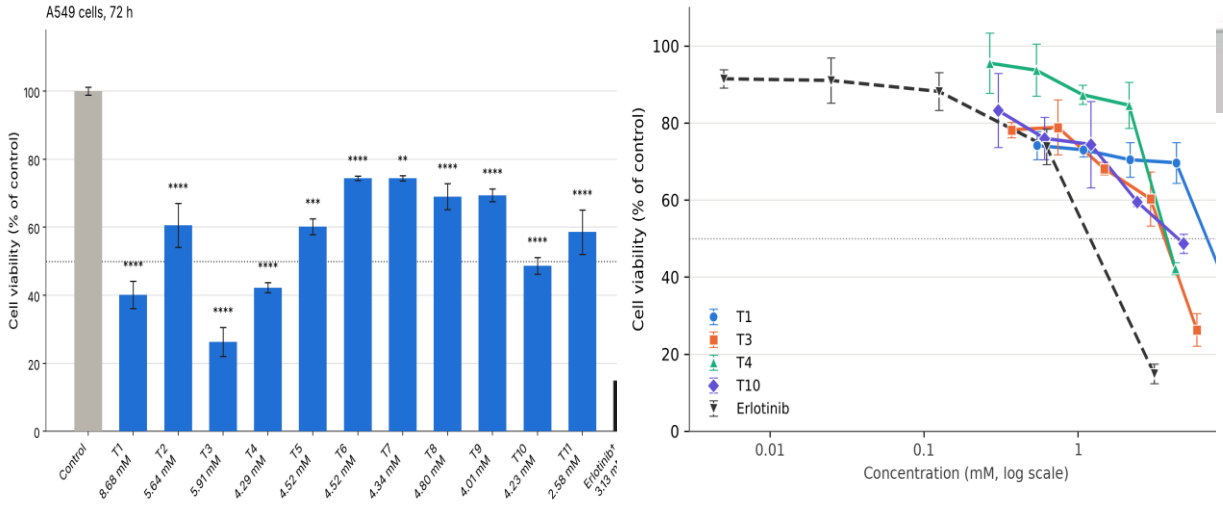
Every analogue reduced A549 viability in a concentration-dependent manner across the tested range, which corresponded to approximately 1.61–8.694 mM depending on molecular weight (Table 3, Figure 3). At the top of the range, viability fell to between 26.30% (T3) and 74.41% (T6). Four analogues crossed the 50% threshold - T3, T1, T4 and T10 — with IC_{50} values of 4.12, 7.67, 3.97 and 3.98 mM respectively (Figure 3b). Erlotinib was largely inert up to 1.25 mM (88.17–91.45% viability), fell to 73.82% at 6.25 mM and to 14.87% at 3.13 mM, giving an IC_{50} of 1.67 mM. Control monolayers were confluent and spindle-shaped, whereas treated wells contained fewer cells, many rounded and shrunken (Figure 3c).

T4 was the most active compound (IC_{50} 3.96 mM), about 2.4-fold less potent than erlotinib, followed closely by T10 (3.98 mM), T3 (4.12 mM) and T1 (7.67 mM). This order broadly followed the docking scores, T4 and T3 being among the top three binders. T11 was the exception: its strong docking score (−9.44 kcal/mol) did not translate into cellular activity, plausibly because of its poor predicted aqueous solubility (ESOL log *S* −5.24) and low predicted gastrointestinal absorption.

Table 3. Cytotoxicity of thiadiazole series against A549 cells (MTT assay, 72 h).

Compound	MW (g/mol)	Cell viability at 1000 µg/mL (%, mean ± SD)	IC_{50} (µg/mL)	IC_{50} (mM)
T1	115.16	40.10 ± 3.97	882.85	7.67
T2	177.23	60.56 ± 6.45	> 1000	> 5.63
T3	169.13	26.30 ± 4.26	696.17	4.12
T4	233.33	42.23 ± 1.53	923.90	3.96
T5	221.24	60.17 ± 2.31	> 1000	> 4.52
T6	221.24	74.41 ± 0.66	> 1000	> 4.52
T7	230.29	74.34 ± 0.77	> 1000	> 4.33
T8	208.24	68.97 ± 3.83	> 1000	> 4.81
T9	249.29	69.39 ± 1.91	> 1000	> 4.01
T10	236.25	48.67 ± 2.49	938.93	3.98
T11	387.52	58.55 ± 6.51	> 1000	> 2.57
Erlotinib	393.44	14.87 ± 2.55 [a]	654.83	1.67

Note: viability is given as a percentage of untreated control (n = 3). IC_{50} values were fitted by non-linear regression (GraphPad Prism) for compounds falling below 50% within 62.5–1000 µg/mL; ">" denotes an IC_{50} not reached at 1000 µg/mL. a Erlotinib was run separately (1 × 104 cells/well, 1.97–1229.5 µg/mL, i.e. 5–3125 µM); the figure shown is viability at 1229.5 µg/mL. The molar values were derived from the listed molecular weights



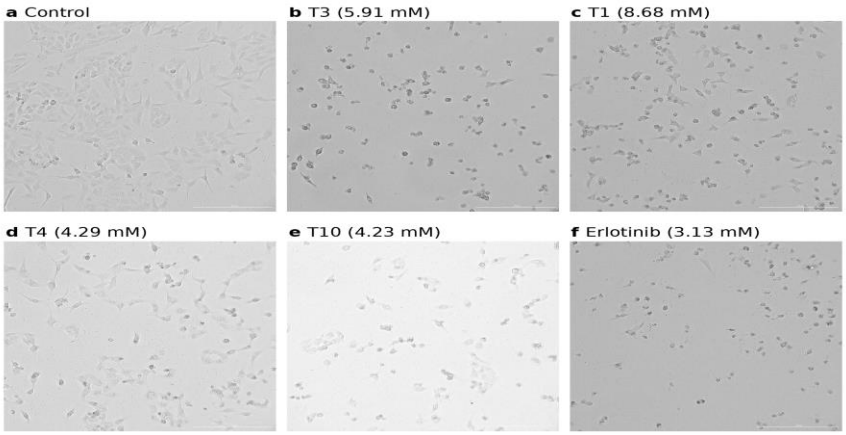


Figure 3. Cytotoxicity of the 1,3,4-thiadiazole analogues against A549 cells after 72 h. (a) Cell viability after treatment with each analogue at the molar concentration given beneath its label and with erlotinib (†) at 3.13 mM; data are mean ± standard deviation (n = 3), compared with the untreated control by one-way analysis of variance with Dunnett's test (**$p < 0.01$, ***$p < 0.001$, ****$p < 0.0001$). (b) Concentration–response curves for the most active analogues T1, T3, T4 and T10 and for erlotinib. In (a) and (b) the dotted line marks 50% viability. (c) Representative phase-contrast images (20×): untreated control and cells treated with T3, T1, T4 and T10 at the concentrations given in (a) and with erlotinib at 3.13 mM.

Overall, the series is weakly cytotoxic, with IC_{50} values in the millimolar range. A549 carries wild-type EGFR alongside an activating KRAS mutation and is a recognized poor responder to EGFR tyrosine kinase inhibitors, so while the data establish dose-dependent killing, they cannot on their own pin that killing on EGFR inhibition. The mismatch between docking score and cellular potency, sharpest for T11, points instead to solubility, membrane permeation, efflux and metabolic stability as the factors limiting this series. T4 and T3 remain the most promising starting points for optimization.

4. CONCLUSION

The 1,3,4-thiadiazole series was deisgned based on the heterocyclic features of fourth-generation EGFR inhibitors, eleven analogues were synthesized, evaluated computationally and on A549 cell line. All eleven docked into the ATP-binding site of EGFR with predicted binding energies more favorable than redocked erlotinib, and each formed the hinge hydrogen bond to Met769 that characterizes ATP-competitive EGFR inhibitors. All complied with Lipinski's rule of five, and all but T11 were predicted to be well absorbed from the gastrointestinal tract. Against A549 cells, however, cytotoxicity was modest: only T3, T1, T4 and T10 reduced viability below 50% at 1000 µg/mL, and on a molar basis the most active analogue wasT4 withIC_{50} value of 3.96 mM), which was about 2.4-fold weaker than erlotinib (1.66 mM). As the A549 human lung adenocarcinoma cell line is normally employed for non-small lung cancer and carries a wild-type EGFR and an activating KRAS mutation, these data do not establish that the observed cytotoxicity arises from EGFR inhibition; cell-free kinase assays and testing in EGFR-mutant lines are required to confirm the mechanism. The 5-(4-*tert*-butylphenyl) analogue T4 and the 5-trifluoromethyl analogue T3 are the most promising starting points for structural optimization of this scaffold for non-small lung cancer

Funding Sources

The author(s) received no financial support for the research, authorship and/or publication of this article.

Data Availability Statement

This article includes all data generated and analyzed during this study. Additional datasets are available from the corresponding author on reasonable request.

Ethics Approval Statement

This study did not involve human participants or animals. All experimental work was carried out *in silico*, by chemical synthesis, and on the established A549 human lung adenocarcinoma cell line; ethical approval and informed consent were therefore not required.

Informed Consent Statement

Not applicable, as the study did not involve human participants.

Clinical Trial Registration

Not applicable.

Author Contributions

Author 1: conceptualization, ligand design, molecular docking and *in silico* ADME studies, synthesis and characterization, cytotoxicity evaluation, data analysis, writing of the original draft.

Author 2 (corresponding author): ideation, conceptualization, supervision, methodology validation, project administration, critical review and editing of the manuscript. Both authors have read thoroughly and approved the final version of the manuscript.

REFERENCES

1. Sung H., Ferlay J., Laversanne M., Siegel R. L., Soerjomataram I. and Jemal A. Global cancer statistics 2024: GLOBOCAN estimates of incidence and mortality worldwide for 34 cancers in 186 countries. CA Cancer J. Clin., 2026; doi:10.3322/caac.70090.
2. Herbst R. S., Morgensztern D. and Boshoff C. The biology and management of non-small cell lung cancer. Nature, 2018; 553(7689): 446-454.

3. International Agency for Research on Cancer. Global Cancer Observatory: Cancer Today. India fact sheet (GLOBOCAN 2024). Lyon: IARC; 2026. Available from: https://gco.iarc.who.int/media/globocan/factsheets/populations/356-india-fact-sheet.pdf [Accessed 21 October 2026].
4. Yarden Y. and Sliwkowski M. X. Untangling the ErbB signalling network. Nat. Rev. Mol. Cell Biol., 2001; 2(2): 127-137.
5. Sharma S. V., Bell D. W., Settleman J. and Haber D. A. Epidermal growth factor receptor mutations in lung cancer. Nat. Rev. Cancer, 2007; 7(3): 169-181.
6. Kobayashi S., Boggon T. J., Dayaram T., Jänne P. A., Kocher O., Meyerson M., et al. EGFR mutation and resistance of non-small-cell lung cancer to gefitinib. N. Engl. J. Med., 2005; 352(8): 786-792.
7. Thress K. S., Paweletz C. P., Felip E., Cho B. C., Stetson D., Dougherty B., et al. Acquired EGFR C797S mutation mediates resistance to AZD9291 in non-small cell lung cancer harboring EGFR T790M. Nat. Med., 2015; 21(6): 560-562.
8. Su C. and Sun S. Y. Fourth-generation epidermal growth factor receptor-tyrosine kinases inhibitors: hope and challenges. Transl. Cancer Res., 2024; 13(8): 3929-3934.
9. Jia Y., Yun C. H., Park E., Ercan D., Manuia M., Juarez J., et al. Overcoming EGFR(T790M) and EGFR(C797S) resistance with mutant-selective allosteric inhibitors. Nature, 2016; 534(7605): 129-132.
10. Giard D. J., Aaronson S. A., Todaro G. J., Arnstein P., Kersey J. H., Dosik H., et al. In vitro cultivation of human tumors: establishment of cell lines derived from a series of solid tumors. J. Natl. Cancer Inst., 1973; 51(5): 1417-1423.
11. Pao W., Wang T. Y., Riely G. J., Miller V. A., Pan Q., Ladanyi M., et al. KRAS mutations and primary resistance of lung adenocarcinomas to gefitinib or erlotinib. PLoS Med., 2005; 2(1): e17.
12. Sos M. L., Michel K., Zander T., Weiss J., Frommolt P., Peifer M., et al. Predicting drug susceptibility of non-small cell lung cancers based on genetic lesions. J. Clin. Invest., 2009; 119(6): 1727-1740.
13. Stamos J., Sliwkowski M. X. and Eigenbrot C. Structure of the epidermal growth factor receptor kinase domain alone and in complex with a 4-anilinoquinazoline inhibitor. J. Biol. Chem., 2002; 277(48): 46265-46272.
14. Maier J. A., Martinez C., Kasavajhala K., Wickstrom L., Hauser K. E. and Simmerling C. ff14SB: improving the accuracy of protein side chain and backbone parameters from ff99SB. J. Chem. Theory Comput., 2015; 11(8): 3696-3713.
15. Wang J., Wolf R. M., Caldwell J. W., Kollman P. A. and Case D. A. Development and testing of a general amber force field. J. Comput. Chem., 2004; 25(9): 1157-1174.
16. Amelia T., Kartasasmita R. E., Ohwada T. and Tjahjono D. H. Structural insight and development of EGFR tyrosine kinase inhibitors. Molecules, 2022; 27(3): 819.
17. Daina A., Michielin O. and Zoete V. SwissADME: a free web tool to evaluate pharmacokinetics, drug-likeness and medicinal chemistry friendliness of small molecules. Sci. Rep., 2017; 7: 42717.
18. Noolvi M. N., Patel H. M., Kamboj S. and Cameotra S. S. Synthesis and antimicrobial evaluation of novel 1,3,4-thiadiazole derivatives of 2-(4-formyl-2-methoxyphenoxy) acetic acid. Arab. J. Chem., 2016; 9(Suppl 2): S1283-S1289.
19. Bait S. P. and Gurjar A. S. Quality by design-based method to synthesize sulfonamides using LiOH·H2O. J. Sulfur Chem., 2025; doi:10.1080/17415993.2025.2543801.